

Electron Momentum Spectroscopy*

I. E. McCarthy

Institute for Atomic Studies, The Flinders University of South Australia,
Bedford Park, S.A. 5042.

Abstract

For sufficiently high electron energies (greater than a few hundred eV) and sufficiently low recoil momenta (less than a few atomic units) the differential cross section for the non-coplanar symmetric (e, 2e) reaction on an atom or molecule depends on the target and ion structure only through the target-ion overlap. Experimental criteria for the energy and momentum are that the apparent structure information does not change when the energy and momentum are varied. The plane-wave impulse approximation is a sufficient description of the reaction mechanism for determining spherically averaged squares of momentum-space orbitals for atoms and molecules and for coefficients describing initial- and final-state correlations. For mainly uncorrelated initial states, spectroscopic factors for final states belonging to the same manifold are uniquely determined. For molecules, summed spectroscopic factors can be compared for different ion manifolds. For atoms, summed spectroscopic factors and higher-momentum profiles require the distorted-wave impulse approximation.

1. Introduction

This paper is about the relationship of the non-coplanar symmetric (e, 2e) reaction (McCarthy and Weigold 1976) to quantum chemistry. It is a very direct relationship and we will see how this comes about and illustrate it with pertinent examples.

Throughout, some terms will be used in senses related to experiment which are described schematically in Fig. 1. The energy E is defined as

$$E = E_A + E_B = E_0 - \epsilon_f, \quad (1)$$

and the momentum p is

$$p = k_A + k_B - k_0. \quad (2)$$

The separation energy ϵ_f of the electronic state of the final ion and the ion recoil momentum p are directly measured by experiment as is the relative differential cross section, spherically averaged over target orientations:

$$\frac{d^5\sigma}{d\Omega_A d\Omega_B dE_A} = (2\pi)^4 \frac{k_A k_B}{k_0} (4\pi)^{-1} \int d\hat{p} |T_f|^2, \quad (3)$$

* Paper presented at the Specialist Workshop on Excited and Ionised States of Atoms and Molecules, Strathgordon, Tasmania, 3-7 February 1986.

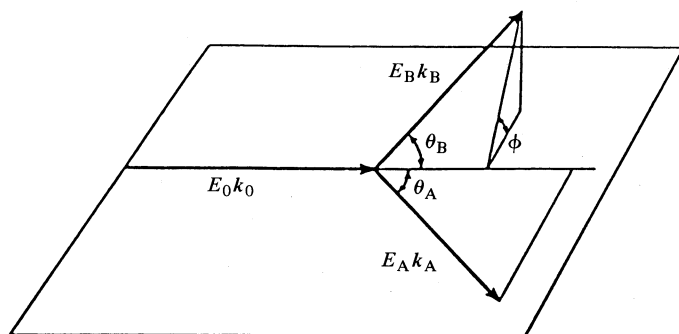


Fig. 1. Schematic diagram defining the kinematic variables used in the description of the $(e, 2e)$ reaction.

where T_f is the amplitude for an $(e, 2e)$ reaction leaving the ion in a state f . The momentum profile is the shape of the curve of the differential cross section plotted against the ion recoil momentum p . The polar angle θ is the angle made by each of k_A and k_B with the incident direction \hat{k}_0 . It is close to 45° to maximise the momentum transfer and minimise p when k_0 , k_A and k_B are coplanar. The azimuthal angle ϕ is the azimuthal angle of k_B relative to the $k_0 k_A$ plane. This is varied from 0° to about 30° in order to vary p from 0 to 2 or 3 a.u. (called low momentum) at energies E of the order of 1 keV (called high energy, since it is many times ϵ_f for the valence states under consideration).

A quantum chemist is a person who believes in the Schrödinger equation and that if the methods, such as variational calculations, configuration interaction (CI) and Green's functions, are used hard enough and long enough all will be revealed. Unfortunately the $(e, 2e)$ reaction cannot be treated by these methods. We cannot even begin to solve the Schrödinger equation because we do not know the boundary conditions for three bodies with Coulomb interactions. This is why some quantum chemists find it difficult and mysterious. Yet I believe that the high-energy low-momentum $(e, 2e)$ reaction is understood better than any other reaction in atomic or nuclear physics in the sense that we can calculate right answers with more certainty. This is not because we reaction theorists are computational geniuses, but it is because the experimentalist has done nearly all the work. He measures enough simultaneous quantities to enable us to focus our thoughts on a kinematic range where quite a simple treatment of the reaction based on an understanding of probability amplitudes is sufficient. This simple treatment relates the reaction very directly to the quantum chemical structure of the target atom or molecule and the ion. Perhaps more importantly the experimentalist can verify the validity of the relationship by checking that the apparent structure information is independent of energy and hence of that part of the calculation dependent on the reaction conditions.

2. Intuitive Reaction Theory

The amplitude for an $(e, 2e)$ reaction leading from the target ground state g to a final ion state f is

$$T_f(k_0, k_A, k_B) = \langle k_A k_B f | T | g k_0 \rangle, \quad (4)$$

where T is the (unknown) transition operator that gives the correct amplitude. We first make a simple and experimentally verifiable approximation.

Binary-encounter Approximation

The transition operator T is approximated by a three-body operator depending on the coordinates of the incident and struck electrons and the centre-of-mass of the residual ion, but not explicitly on the coordinates of the remaining electrons. With this approximation the (e, 2e) amplitude becomes

$$T_f(k_0, k_A, k_B) = \int d^3q \langle k_A k_B | T | q k_0 \rangle \langle qf | g \rangle. \quad (5)$$

The vitally important feature about the form (5) is that T_f now depends on the structure wavefunctions f of the ion and g of the target ground state only through the target-ion overlap $\langle qf | g \rangle$. This quantity is directly calculated by the methods of quantum chemistry, so that (5) constitutes the relationship between the reaction and quantum chemistry. Its verification depends on whether apparent structure information is independent of energy E .

We can form an *a priori* idea of the conditions for the validity of (5). Some of the terms it neglects are exchange terms involving the overlap of a continuum and a bound-state orbital for a particular electron. These overlaps are vanishingly small for electron energies of several hundred eV and valence orbitals. This gives a lower limit on E .

The first amplitude in the integrand of (5) describes the reaction mechanism. We must make further approximations to it in order to calculate the differential cross section. The simplest approximation is that T just describes the collision of the two electrons. It then becomes the electron-electron t -matrix:

$$\langle k_A k_B | T | q k_0 \rangle = \langle k' | t(E) | k \rangle \delta(q - k_A - k_B + k_0), \quad (6)$$

where

$$k' = \frac{1}{2}(k_A - k_B), \quad k = \frac{1}{2}(q - k_0), \quad q = p.$$

This is the plane-wave impulse approximation (PWIA). We note that (5) now factorises into the target-ion overlap $\langle pf | g \rangle$ calculated at the experimental momentum p and an electron-electron collision factor which is essentially the Mott scattering amplitude except that k' corresponds to the experimental energy E but k does not. It is half-off-shell, but all momenta are measured in the experiment. When summed and averaged over electron spin states the electron-electron factor in the cross section becomes (Chen and Chen 1972)

$$f_{ee} = \frac{1}{(2\pi^2)^2} \frac{2\pi\nu}{\exp(2\pi\nu) - 1} \left\{ \frac{1}{|k_0 - k_A|^4} + \frac{1}{|k_0 - k_B|^4} - \frac{1}{|k_0 - k_A|^2} \frac{1}{|k_0 - k_B|^2} \right. \\ \left. \times \cos\left(\nu \ln \frac{|k_0 - k_B|^2}{|k_0 - k_A|^2}\right) \right\}, \quad (7)$$

where $\nu = 1/|k_A - k_B|$, and the cross section is

$$\frac{d^5\sigma}{d\Omega_A d\Omega_B dE_A} = (2\pi)^4 \frac{k_A k_B}{k_0} f_{ee} (4\pi)^{-1} \int d\hat{p} |\langle pf | g \rangle|^2. \quad (8)$$

In fact we expect that momentum can be transferred by elastic scattering in each two-electron subsystem (i.e. the electron waves undergo distortion from the plane-wave description). It is computationally feasible to take this into account by retaining the factorisation implied by (6) but replacing the plane waves $|k_A\rangle$, $|k_B\rangle$ and $|k_0\rangle$ in $\langle qf|g\rangle$ by elastic scattering states $|\chi^{(-)}(k_A)\rangle$, $|\chi^{(-)}(k_B)\rangle$ and $|\chi^{(+)}(k_0)\rangle$ calculated in the appropriate two-body potential. In fact we use the static-exchange potential of one electron and the ion for the final state and that of one electron and the target for the initial state. This gives us the distorted-wave impulse approximation (DWIA)

$$\frac{d^5\sigma}{d\Omega_A d\Omega_B dE_a} = (2\pi)^4 \frac{k_A k_B}{k_0} f_{ee} \times (4\pi)^{-1} \int d\hat{p} |\langle \chi^{(-)}(k_A) \chi^{(-)}(k_B) f | g \chi^{(+)}(k_0) \rangle|^2, \quad (9)$$

which is the reaction theory that gives a complete understanding of the reaction under the high-energy low-momentum conditions of electron momentum spectroscopy for atomic targets. For molecular targets it is difficult to calculate the distorted waves, but our complete understanding enables us to identify experimental conditions under which the PWIA (8) is valid and gives the same structure information.

3. Comparison with Photoelectron Spectroscopy

In considering the comparison of electron momentum spectroscopy (EMS) with photoelectron spectroscopy (PES) it is appropriate at this stage to make some comparisons for reactions in which (e, 2e) is experimentally feasible (McCarthy 1985). At present this covers stable gas targets and an energy resolution ΔE of approximately 1 eV. Solid or transient-gas targets and higher energy resolution are at present the exclusive province of PES, although this is changing.

It is sometimes claimed that PES gives valuable structure information about valence states. Indeed there is a superficial resemblance to EMS in that both observe the energies of electronic states of the ion; however, here the resemblance ends. PES obviously contains structure information, but it is in a very convoluted form involving a heroic computational effort to describe differential cross sections that, for the spectroscopic application, are only now beginning to be reliably measured.

The major theoretical problem with describing photoionisation is inherent in the two-body kinematics of the reaction. The photoelectron energy E is uniquely related to the momentum by

$$E = \frac{1}{2}p^2. \quad (10)$$

Thus the high-energy low-momentum condition is unattainable in PES. The reaction involves a difficult (but possible) calculation at low energy, using a continuum electron function (not a plane wave) derived from a calculation involving channel coupling and electron correlation (e.g. Berrington *et al.* 1980). However, at high energy and momentum (for example, $p \sim 10a_0^{-1}$ in X-ray photoelectron spectroscopy) the plane-wave approximation for the continuum electron is invalidated by the strong short-distance electron-ion potential and there is a new amplitude in the calculation, beyond the usual dipole approximation, that becomes non-negligible at such momenta (Amusia and Kheifets 1985).

4. One-electron Chemistry

The $(e, 2e)$ reaction is a direct observation of the target-ion overlap $\langle pf|g\rangle$, under the conditions of validity of the PWIA. Under conditions that are realistic for most targets it takes a particularly simple form.

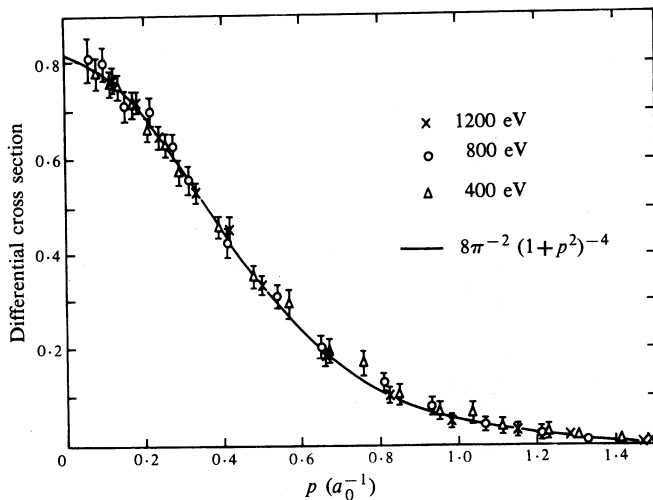


Fig. 2. The momentum profile at different energies for the $(e, 2e)$ reaction on the hydrogen atom (Lohmann and Weigold 1981). The differential cross section is arbitrarily normalised.

For the hydrogen atom the overlap is

$$|\langle pf|g\rangle|^2 = |\phi(p)|^2 = 8\pi^{-2}(1+p^2)^{-4}. \quad (11)$$

This momentum profile is verified (Lohmann and Weigold 1981) for different energies in Fig. 2, thus verifying the validity of the assumptions involved in the PWIA (8).

For the helium atom (Cook *et al.* 1984) the overlap can be fully evaluated very easily by using a converged CI wavefunction for g and the (hydrogenic) wavefunctions of He^+ . For the $1s$ state the momentum profile is the same as that obtained using the He Hartree-Fock function as an approximation to $\langle pf|g\rangle$ over several orders of magnitude. Initial-state correlations result in excitation of $n = 2$ and higher states of He^+ . The $n = 2$ momentum profile relative to the $1s$ profile is shown in Fig. 3.

For larger targets we represent $|g\rangle$ as a CI expansion in Slater determinants $|\alpha\rangle$ of target Hartree-Fock orbitals:

$$|g\rangle = \sum_{\alpha} a_{\alpha} |\alpha\rangle. \quad (12)$$

In order to use orthonormality we also represent the ion in terms of target Slater determinants $|\beta\rangle$ coupled with appropriate symmetry to one-hole states ϕ_j , whose symmetry is indicated by a quantum number set j . Final ion states f_m belonging to a symmetry manifold indicated by m are expanded as

$$|f_m\rangle = \sum_{j\beta} t_{j\beta}^{(f)} C_{jm\beta} \phi_j^{\dagger} |\beta\rangle. \quad (13)$$

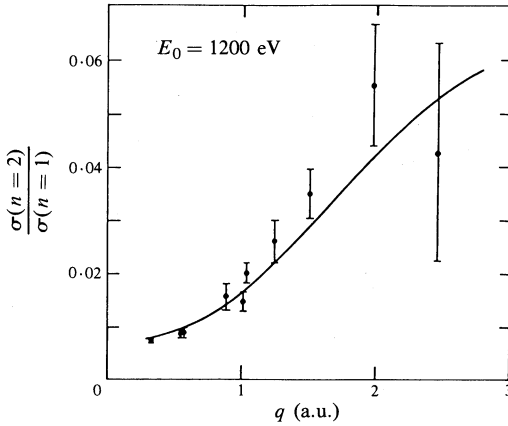


Fig. 3. The ratio of $n = 2$ to $n = 1$ cross sections for the $(e, 2e)$ reaction on helium compared with the PWIA (solid curve) using a converged CI function for the ground state (Mitroy *et al.* 1985; Cook *et al.* 1984).

We normally consider final states belonging to a particular symmetry manifold m and thus drop the subscript m from f .

In the common case of $a_0 \sim 1$ for closed-shell targets in which there is very little initial-state correlation, the overlap is

$$\langle pf | g \rangle = N^{\frac{1}{2}} t_{j0}^{(f)} \psi_j(\mathbf{p}), \quad (14)$$

where orbitals with the same symmetry j sum to a function $\psi_j(\mathbf{p})$ called the characteristic orbital. As in the case of helium, $\psi_j(\mathbf{p})$ is essentially a target Hartree-Fock orbital. The factor $N^{\frac{1}{2}}$, where N is the occupation number of the target orbital ψ_j , is introduced by antisymmetrisation (Cook *et al.* 1986). The square of the spectroscopic amplitude $t_{j0}^{(f)}$ is the spectroscopic factor $S_j^{(f)}$. It represents the probability that f consists of the one-hole configuration $\psi_j^\dagger | 0 \rangle$.

The spectroscopic sum rule

$$\sum_f S_j^{(f)} = 1, \quad (15)$$

obtained from the orthonormality and closure relations for the manifold defined by the symmetry j , enables us to make a one-electron theory of the $(e, 2e)$ reaction which amounts to an experimental definition of an orbital for a manifold j :

- (i) The orbital momentum profile $\int d\hat{p} |\psi_j(\mathbf{p})|^2$ is given by the $(e, 2e)$ profile. We note that for EMS f_{ee} is essentially independent of p .
- (ii) The magnitude of the orbital differential cross section is given by the sum of cross sections for reactions to states f in the manifold j .
- (iii) The orbital energy is obtained from the orthonormality and closure relations as the manifold centroid

$$\epsilon_j = \sum_f S_j^{(f)} \epsilon_f. \quad (16)$$

5. The Understanding Afforded by the DWIA

If we make the approximation that the target ground state $|g\rangle$ can be represented by the target Hartree–Fock determinant $|0\rangle$, we can substitute the one-electron overlap (14) into the expression (9) to obtain the target Hartree–Fock DWIA (THF-DWIA):

$$\frac{d^5\sigma}{d\Omega_A d\Omega_B dE_A} = (2\pi)^4 \frac{k_A k_B}{k_0} f_{ee} N S_j^{(f)} \times (4\pi)^{-1} \int d\hat{p} |\langle \chi^{(-)}(k_A) \chi^{(-)}(k_B) | \psi_j \chi^{(+)}(k_0) \rangle|^2. \quad (17)$$

We note that the THF approximation involves the neglect of initial-state correlation effects, which we illustrated for helium in Fig. 3. They are usually of the order of a few per cent.

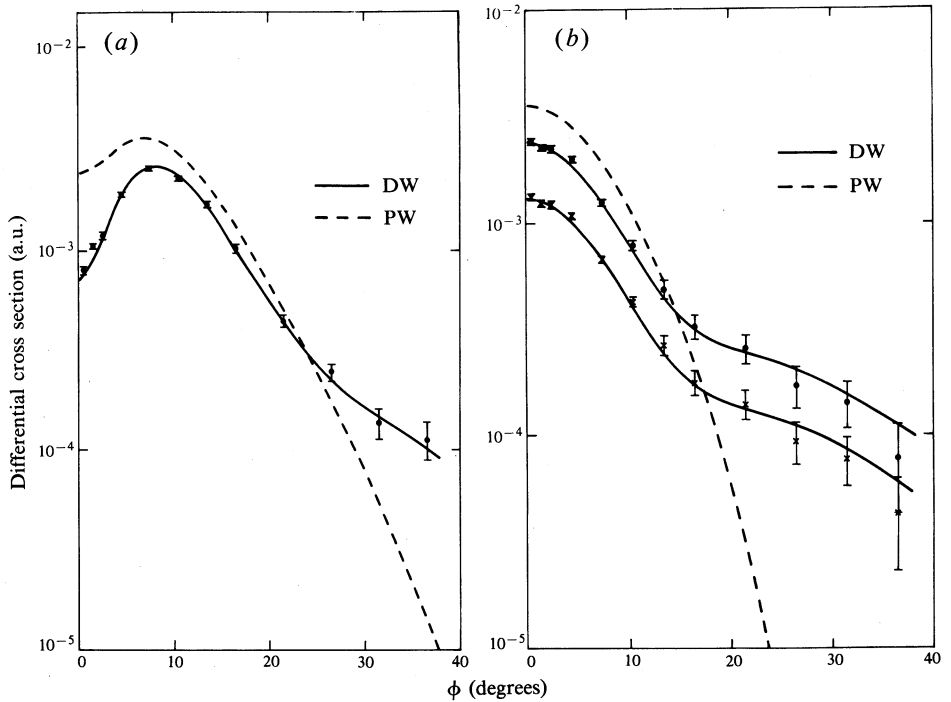


Fig. 4. The DWIA and PWIA compared with 1000 eV ($e, 2e$) data at $\theta = 47^\circ$ for (a) the 3p orbital of Ar^+ (McCarthy and Weigold 1985) and (b) the 29.3 eV state of Ar^+ (crosses) and the 3s manifold sum (closed circles). The experimental points are normalised to the curve at 7.5° in both plots. In (b) the DWIA curve for the 29.3 eV state includes a spectroscopic factor of 0.55 (McCarthy and Weigold 1985).

Fig. 4a shows the 3p manifold of Ar^+ , which involves negligible final-state correlations. The THF-DWIA agrees perfectly with the experimental cross section (normalised at 7.5°). We note that the polar angle θ in this experiment is 47° . The theoretical description is good here, even though the small- ϕ shape of the PWIA is not correct in detail for the 3p profile. This case is chosen first, since it illustrates the

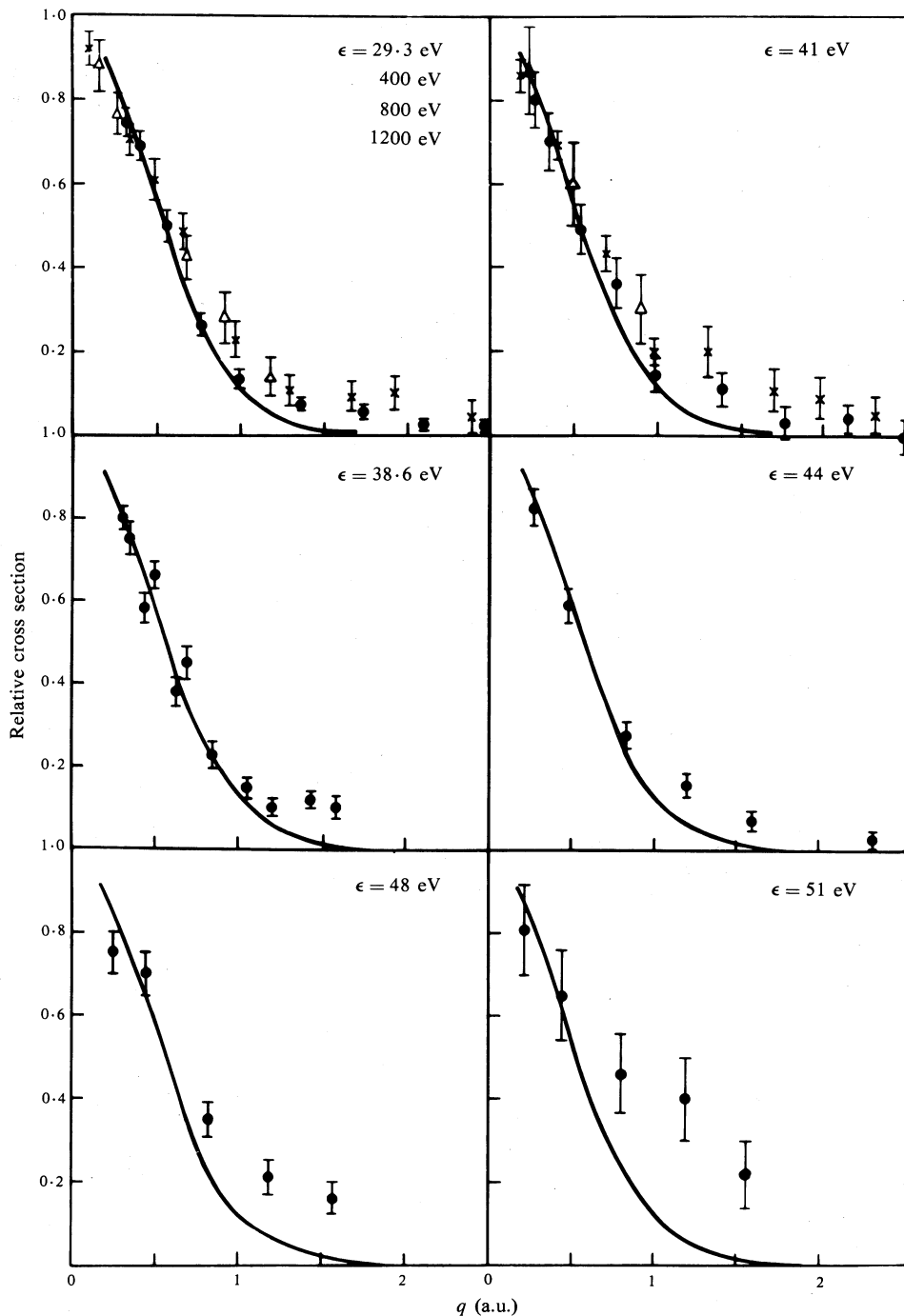


Fig. 5. Momentum profiles for different ion states in the 3s manifold for the $(e, 2e)$ reaction on argon at the indicated energies (McCarthy and Weigold 1976). The curve in each case is the 3s Hartree-Fock PWIA.

excellent understanding of the reaction achieved by the DWIA, independent of whether the PWIA is correct. In fact for $\theta = 45^\circ$ the PWIA achieves excellent agreement with experiment at small angles for argon and other noble gases (Leung and Brion 1983). This case is discussed in detail for xenon below.

Fig. 4*b* for the 3*s* manifold illustrates the full power of the DWIA analysis. Not only is the profile shape correct, but so too is its magnitude (remembering that the whole experiment has already been normalised as for Fig. 4*a*). The spectroscopic factor $S_{3s}^{(29.3)}$ of the strongest state at 29.3 eV is found to be 0.55 ± 0.02 by two independent methods, i.e. by use of the sum rule (15) within the 3*s* manifold and by direct comparison of the 29.3 eV cross section with the 3*p* cross section. We note that the low-momentum shape of the 3*s* profile is given adequately by the PWIA. This has been used to assign spectroscopic factors within the 3*s* manifold. Momentum profiles for 3*s* states are shown in Fig. 5.

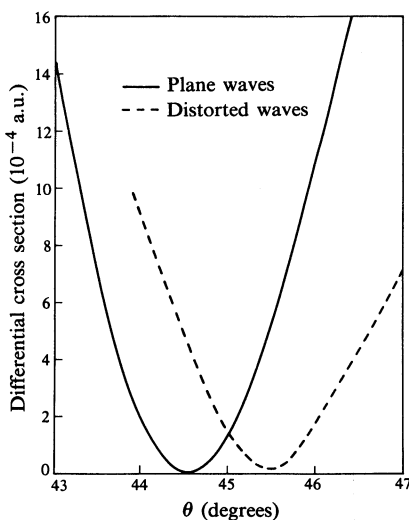


Fig. 6. The PWIA and DWIA for the 1000 eV (*e*, 2*e*) reaction on argon for $\phi = 0$ and varying θ near the low-momentum minimum.

We can find the optimum polar angle θ for the PWIA by considering the cross section in the $\phi = 0$ plane as a function of θ . This is illustrated by calculations shown in Fig. 6 for the Ar 3*p* case. The plane-wave minimum is shifted to the left of 45° by the finite separation energy. The distorted-wave minimum is shifted to the right by about the same amount since the average distorting potential is comparable with the separation energy. The plane-wave and distorted-wave cross sections agree at 45° . This argument holds approximately for all orbitals so the optimum angle for the PWIA is 45° . The angle θ is therefore best chosen at 45° for EMS studies of molecules in non-coplanar symmetric geometry, since distorted-wave treatments for molecular targets are as yet impractical.

Fig. 7 (for $\theta = 45^\circ$) compares the 5*p* and 5*s* manifolds of xenon, analogous to Fig. 4 for argon. Here the Dirac-Fock orbitals are used in preference to Hartree-Fock, in view of the fact that relativistic effects are expected to be important for xenon. Fig. 8 shows that the correct ratio of 5*p*_{3/2} to 5*p*_{1/2} cross sections is obtained. The one-electron analysis is completely confirmed. In addition the PWIA and DWIA agree in shape detail up to $p \sim 1.5 a_0^{-1}$ for 5*p* and $1.0 a_0^{-1}$ for 5*s*, both of which are

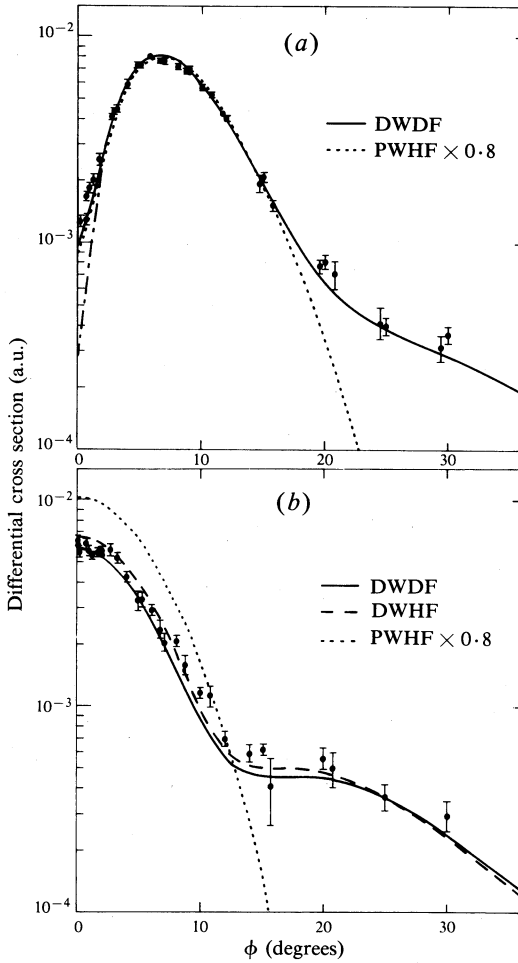


Fig. 7. The DWIA and PWIA compared with 1000 eV (e,2e) data at $\theta = 45^\circ$ for (a) the summed 5p orbitals of xenon (Cook *et al.* 1986) and (b) the 5s manifold sum of xenon. The experimental points are normalised to the 5p DWDF curve at 5° in both plots.

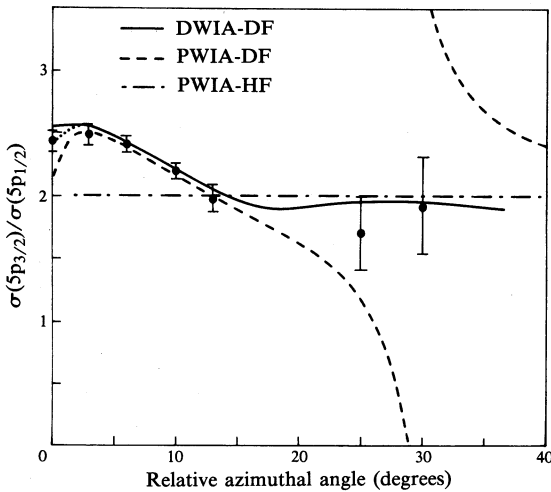


Fig. 8. The DWIA and PWIA calculations of the ratio of $5p_{3/2}$ to $5p_{1/2}$ cross sections for the 1000 eV (e,2e) reaction on xenon (Cook *et al.* 1986).

sufficiently large momenta for the main features of the profiles to be observed, and in particular for assignment of manifold symmetry. This comparison study for xenon affords a convincing verification of the use of the PWIA at $\theta = 45^\circ$ to give detailed low-momentum profiles.

Final confirmation of the one-electron analysis is given by the orbital energy (16) of the argon 3s manifold, which is 34.5 ± 0.2 eV in agreement with the Hartree-Fock value, and of the xenon 5s manifold, which is 27.6 ± 0.3 eV in agreement with the Dirac-Fock value (27.5 eV).

6. The PWIA for Molecules

The understanding of the $(e, 2e)$ reaction that we have obtained for atoms leads to the conclusion that the optimum conditions for the use of the PWIA for molecules are $E \sim 1000$ eV and $\theta = 45^\circ$ in non-coplanar symmetric geometry.

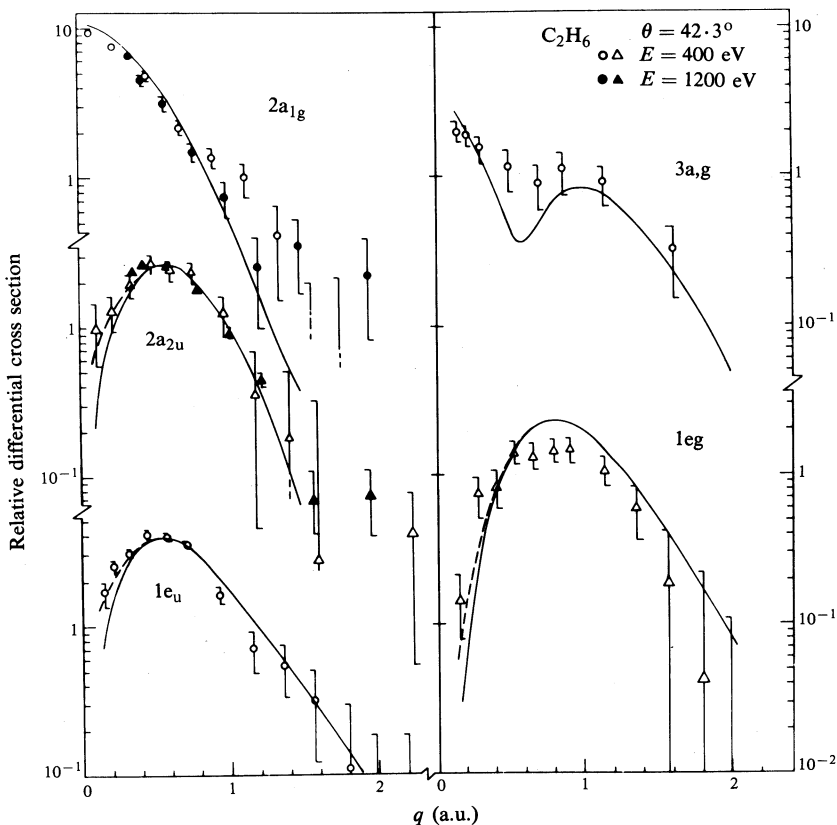


Fig. 9. Momentum profiles for the valence orbitals of ethane analysed with the PWIA and Hartree-Fock functions (Dey *et al.* 1976).

Fig. 9 for ethane illustrates the main features of the one-electron THF-PWIA analysis. Here only a single point normalisation on one orbital is used in the comparison of theory and experiment. First the summed manifold momentum profiles all agree with experiment in relative magnitude, indicating that spectroscopic factor

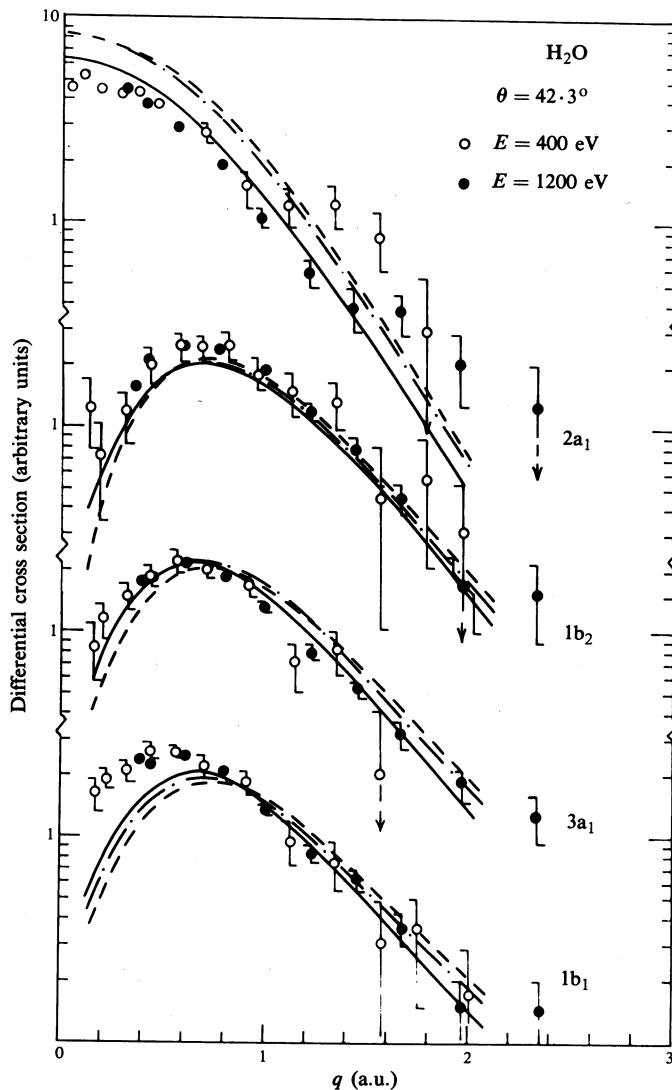


Fig. 10. Momentum profiles for the valence orbitals of water compared with the PWIA using different calculations of $\langle qf|g\rangle$ (Dixon *et al.* 1977). The solid curve is the overlap amplitude calculated by using Green's function. Broken curves are for molecular orbitals with different basis sets.

assignments within manifolds are confirmed by comparing manifold sums. It is of course not necessary to measure the one unknown value that would make cross sections absolute. Absolute normalisation is done by the spectroscopic sum rule. The analysis is valid for $E = 400$ eV and 1200 eV up to maximum momenta p_{\max} that vary with E and the manifold. For example p_{\max} is $0.9a_0^{-1}$ for $2a_{1g}$ at 400 eV and $1.2a_0^{-1}$ at 1200 eV. Taking account of angular resolution improves the small- ϕ agreement.

Fig. 10 for water shows that a direct calculation of the overlap, in this case by using Green's function methods (Dixon *et al.* 1977), improves on profile shapes given

by medium-quality self-consistent field orbitals. The low-momentum disagreement for the $1b_1$ orbital is attributed to inadequate structure calculations in view of the precise agreement for other cases. This is confirmed in considerable detail by Bawagan *et al.* (1985).

7. Correlations within an Inner-valence Manifold

Spectroscopic factors are precisely assigned by EMS to the fragments of an orbital constituting an inner-valence manifold. So far this has provided the toughest challenge to quantum chemistry, and until recently direct CI methods gave only qualitatively correct relative magnitudes while methods using Green's functions have been less successful.

The simplest non-trivial test case is the 3s manifold of argon, since the fragments are well-separated and precisely assigned (see Fig. 5). Large-basis direct CI calculations by Mitroy *et al.* (1984) obtained 0.65 for the largest spectroscopic factor in comparison with the experimental value of 0.55 ± 0.02 . A Green's function calculation of the overlap amplitude by Amusia and Kheifets (1985) gave improved spectroscopic factors. The comparison with experiment is given in Table 1.

Table 1. Spectroscopic factors for the 3s manifold of the argon ion

AK, Green's function calculation (Amusia and Kheifets 1985); MAM, direct CI calculation (Mitroy *et al.* 1984); EXP, experimental values (McCarthy and Weigold 1985)

ϵ (eV)	Assignment	AK	MAM	EXP
29.3	$3s3p^6$	0.55	0.651	0.547 ± 0.019
36.7	$3s^23p^44s$	—	0.016	0.032 ± 0.008
38.6	$3s^23p^43d$	0.20	0.176	0.175 ± 0.011
41.2	$3s^23p^44d$	0.11	0.081	0.074 ± 0.007
42–43.4	$3s^23p^45d$	0.04	0.076	0.041 ± 0.006
>43.4	—	—	0.076	0.122 ± 0.008

A recent direct CI calculation by the Perugia group (A. Sgamellotti, personal communication 1986) for Cl_2 involved about 100 000 configurations for the inner-valence manifolds. Separation energies and relative spectroscopic factors agree closely with experiment for the first two of three large fragments of the $4\sigma_u$ manifold that are clearly observable. There are indications that calculations of this order of magnitude are necessary to obtain an adequate quantum-chemical description of the spectroscopic-factor aspect of electron correlations.

References

- Amusia, M. Ya., and Kheifets, A. S. (1985). *J. Phys. B* **18**, L679.
 Bawagan, A. O., Lee, L. Y., Leung, K. T., and Brion, C. E. (1985). *Chem. Phys.* **99**, 367.
 Berrington, K. A., Burke, P. G., Fon, W. C., and Taylor, K. T. (1980). *J. Phys. B* **15**, L603.
 Chen, J. C. Y., and Chen, A. C. (1972). *Adv. Atom. Mol. Phys.* **8**, 71.
 Cook, J. P. D., McCarthy, I. E., Mitroy, J. D., and Weigold, E. (1986). *Phys. Rev. A* **33**, 211.
 Cook, J. P. D., McCarthy, I. E., Stelbovics, A. T., and Weigold, E. (1984). *J. Phys. B* **17**, 2339.
 Dey, S., Dixon, A. J., McCarthy, I. E., and Weigold, E. (1976). *J. Electron Spectrosc.* **9**, 397.
 Dixon, A. J., Dey, S., McCarthy, I. E., Weigold, E., and Williams, G. R. J. (1977). *Chem. Phys.* **21**, 81.
 Leung, K. T., and Brion, C. E. (1983). *Chem. Phys.* **82**, 87.

- Lohmann, B., and Weigold, E. (1981). *Phys. Lett. A* **86**, 139.
- McCarthy, I. E. (1985). *J. Electron Spectrosc.* **36**, 37.
- McCarthy, I. E., and Weigold, E. (1976). *Phys. Rep. C* **27**, 275.
- McCarthy, I. E., and Weigold, E. (1985). *Phys. Rev. A* **31**, 160.
- Mitroy, J. D., Amos, K. A., and Morrison, I. (1984). *J. Phys. B* **17**, 1659.
- Mitroy, J. D., McCarthy, I. E., and Weigold, E. (1985). *J. Phys. B* **18**, 4149.

Manuscript received 13 March, accepted 23 May 1986